Reducing Southern Ocean biases in the FOCI climate model

Joakim Kjellsson[1,2], Sebastian Wahl[1], Sabine Bischof[1], Lasse Kummer[2], Torge Martin[1], Robin Pilch Kedzierski[3,1], Mathias Zeller[1], Malin Ödalen[1], Wonsun Park[4,5]

[1]GEOMAR Helmholtz Centre for Ocean Research Kiel, Germany
[2]Christian-Albrechts-Universität zu Kiel, Germany
[3]Now at: Meteorological Institute, Universität Hamburg, Germany
[4]Center for Climate Physics, Institute for Basic Science (IBS), Busan, Republic of Korea
[5]Department of Climate System, Pusan National University, Busan, Republic of Korea

Key Points:

- Positive SST bias in Southern Ocean is mitigated by reducing oceanic diffusion or reduced coupling time step
- Shorter coupling time step increases Antarctic sea-ice area, weakens Weddell Gyre and intensifies Antarctic Bottom Water cell
- Surface wind biases are not related to SST biases

Corresponding author: Joakim Kjellsson, jkjellsson@geomar.de

Abstract

We explore the sensitivity of Southern Ocean surface and deep ocean temperature and salinity biases in the FOCI coupled climate model to atmosphere-ocean coupling time step and to lateral diffusion in the ocean with the goal to reduce biases common to climate models. The reference simulation suffers from a warm bias at the sea surface which also extends down to the seafloor in the Southern Ocean and is accompanied by a too fresh surface, in particular along the Antarctic coast. Reducing the atmosphere-ocean coupling time step from 3 hours to 1 hour results in increased sea-ice production on the shelf and enhanced melting to the north which reduces the fresh bias of the shelf water while also strengthening the meridional density gradient favouring a stronger Antarctic Circumpolar Current (ACC). With the shorter coupling step we also find a stronger meridional overturning circulation with more upwelling and downwelling south and north of the ACC respectively, as well as a reduced warm bias at almost all depths. Tuning the lateral ocean mixing has only a small effect on the model biases, which contradicts previous studies using a similar model configuration. We note that the latitude of the surface westerly wind maximum has a northward bias in the reference simulation and that this bias is unchanged as the surface temperature and sea-ice biases are reduced in the coupled simulations. Hence, the surface wind biases over the Southern Hemisphere midlatitudes appear to be unrelated to biases in sea-surface conditions.

Plain Language Summary

The Southern Ocean (south of 40°S) plays a large role in shaping the ocean circulation and Earth's climate by hosting a majority of the oceanic heat uptake and being one of the few locations where the atmosphere is in close contact with the deep ocean via the formation of deep water. Unfortunately, the FOCI climate model, as many other climate models, struggles to reproduce the observed state of the Southern Ocean. The sea surface in FOCI is biased toward being too warm and to lack sea ice. We perform a series of model experiments where the coupling time step is changed from the default 3 hours to 2 and 1 hours. The coupling time step defines how often the atmosphere model receives an updated surface state from the ocean model and provides new exchange fluxes for forcing the ocean in return. We find that a shorter coupling time step allows the model to produce more sea ice along the Antarctic coast which increases the sea-ice concentration and reduces biases in temperature and salinity. We also show that the magnitude of lateral mixing in the ocean model has only a small effect on model biases.

1 Introduction

The Southern Ocean plays a major role in setting the global climate by acting as the inter-connection of the Atlantic, Indian and Pacific Ocean (Döös, 1995), and is also one of the few places where deep water can form (Kuhlbrodt et al., 2007). While it comprises only 30% of the global ocean surface area, the Southern Ocean is responsible for 40 % of the anthropogenic CO_2 uptake and 75% of the ocean heat uptake (Frölicher et al., 2015). The ability of climate models to reproduce the observed Southern Ocean state is thus key for reliable climate projections.

Yet, many of the most prominent biases of global climate models participating in the Coupled Model Intercomparison Project phase 6 (CMIP6) and its predecessor CMIP5 occur in the Southern Ocean. Biases are found in e.g. sea-ice cover (Turner et al., 2013; Roach et al., 2020), sea surface temperature (SST) (C. Wang et al., 2014; Y. Wang et al., 2022), zonal wind (Bracegirdle & Marshall, 2012), bottom water properties (Heuzé et al., 2013; Heuzé, 2021) and frequency of deep water formation (Kjellsson et al., 2015; Reintges et al., 2017) with implications for the large-scale ocean circulation (Beadling et al., 2020). Biases in SST have been attributed to biases in cloud radiative effect (Hyder et al., 2018), ocean model horizontal resolution (Hewitt et al., 2016), lateral diffusion (Storkey

et al., 2018) and the representation of ocean vertical mixing (Calvert & Siddorn, 2013). Iso-pycnal diffusion has been shown to play a large role in setting the temperature in Southern Ocean and the subpolar North Atlantic (Hieronymus & Nycander, 2013) which is likely why SST biases in these regions are sensitive to the magnitude of the diffusion coefficient. Sea-ice concentration, SST and bottom-water property biases can be intimately linked as a warm surface in summer causes low sea-ice concentration and thus excessive sea-ice production and deep-water formation in autumn (Heuzé et al., 2013). As oceanic uptake of heat and carbon are sensitive to both SST and surface winds (Rodgers et al., 2014; Yamamoto et al., 2018), biases in these variables make climate-model predictions of anthropogenic climate change less reliable. Biases in Antarctic Circumpolar Current (ACC) strength and width do not seem to be related to biases in the surface westerlies but rather to biases in the meridional density gradient (Meijers et al., 2012; Beadling et al., 2019) with the meridional temperature gradient playing a larger role than that of salinity. In addition, the transport through Drake Passage (often taken as a measure of ACC transport) has a strong dependence on horizontal resolution of the ocean model component where eddy-parameterized models ($\sim 1°$) and eddy-rich models ($\sim 1/10°$) represent the transport reasonably well while eddy-present models ($\sim 1/4°$) underestimate the transport. Indeed, Beadling et al. (2020) showed that climate models HadGEM-GC3, CNRM-CM6 and GFDL-CM4 had weaker Drake Passage transport in versions with an eddy-present ocean ($1/4°$) compared to versions with an eddy-parameterized ocean ($0.5°$-$1°$).

Biases in the latitude of the surface westerly wind maximum over the Southern Ocean were prevalent in almost all models of the CMIP5 although the atmosphere components alone generally achieve more realistic westerlies in the Atmospheric Model Intercomparison Project (AMIP) (Bracegirdle et al., 2013), suggesting that wind biases are likely exacerbated by oceanic feedbacks. Idealized model experiments have revealed a strong sensitivity of the midlatitude westerlies to the surface friction (Chen et al., 2007), where too strong surface friction results in too weak and equatorward-shifted westerlies. There has been a steady improvement in representing Southern Ocean surface winds (Swart & Fyfe, 2012; Bracegirdle et al., 2020) and the ACC from CMIP3 to CMIP6, the latter likely due to increased resolution of ocean bathymetry (Beadling et al., 2020).

The role of the atmosphere-ocean coupling time step for surface biases in climate models is rarely documented. Climate models generally use lagged coupling where e.g. the atmosphere uses the ocean surface state from the last coupling step to compute surface fluxes for the next step, and the coupling time step is often chosen to be 3 hours or less to represent the diurnal cycle. However, it is not clear how sensitive climate-model biases are to the choice of coupling time step, although there are indications that the sensitivity is high in the high latitudes (A. Roberts et al., 2015) due to the presence of sea ice.

In this paper we present a series of sensitivity experiments with the FOCI coupled climate model (Matthes et al., 2020) where both coupling time step and ocean lateral diffusion are altered. Our focus will be on the model biases of temperature, salinity and ocean circulation in the Southern Ocean.

2 Data

2.1 FOCI

We use the Flexible Ocean Climate Infrastructure (FOCI) model version 1 and provide a brief description of the model. The reader is referred to (Matthes et al., 2020) for further details about the model.

The atmosphere model is ECHAM version 6.3.05p2 with spectral truncation of T_q63, a grid-point resolution of $\sim 1.8°$ (~ 200 km) and 95 vertical hybrid sigma-pressure levels (Stevens et al., 2013; Müller et al., 2018a). Land-surface processes, such as atmosphere-

land exchanges of heat and water, are simulated by the JSBACH model (Reick et al., 2013).

The ocean/sea-ice model in FOCI is NEMO version 3.6 (Madec et al., 2016) and LIM2 (Fichefet & Maqueda, 1997). The ocean model version is thus comparable to several other climate models participating in CMIP6 e.g. CNRM-CM6-1 (Voldoire et al., 2019), IPSL-CM6 (Boucher et al., 2020), EC-Earth3 (Döscher et al., 2022), HadGEM-GC3 (Williams et al., 2018), and in particular CMCC-CM (Scoccimarro et al., 2011) which also uses the ECHAM atmosphere model but version 5. The ocean grid is ORCA05 (nominally 0.5° horizontal resolution) with 46 fixed z-levels where vertical resolution varies from 5m near the surface to 200m at depth. The horizontal resolution is not sufficient to be eddy-rich, i.e. explicitly resolve baroclinic instabilities and eddy-mean flow interactions, especially in mid-to-high latitudes. We therefore use a Gent-McWilliams parameterization (GM, (Gent & McWilliams, 1990; Treguier et al., 1997)) to compute an eddy-induced diffusion. The GM diffusivity has an upper limit of 1000 $\mathrm{m}^2\ \mathrm{s}^{-1}$ and is reduced in the tropics (20°S to 20°N) as the model is more capable of resolving ocean eddies in this region. Additionally, we also use iso-neutral Laplacian tracer diffusion with a globally constant coefficient $A_{\mathrm{h,t}} = 600\ \mathrm{m}^2\ \mathrm{s}^{-1}$ to represent other forms of mixing, e.g. submesoscale processes.

Coupling between ocean and atmosphere is done using the OASIS3-MCT2.8 coupler (Craig et al., 2017). The coupling time step is 3 hours, which is a compromise between resolving the diurnal cycle and keeping inter-model communications to a minimum. Many climate models participating in CMIP6 have opted for a somewhat shorter coupling time step e.g. IPSL-CM6A-LR (90 min, Boucher et al. (2020)), HadGEM-GC3 (hourly, Williams et al. (2018)), MPI-ESM-HR (hourly, Müller et al. (2018b)).

2.2 Simulations

We have performed a number of pre-industrial (piControl) experiments where external forcing is fixed at year 1850 levels. Each experiment starts at year 1850 and runs for at least 500 years. We discard the first 200 years as spinup and only analyse the last 300 years, i.e. model years 2050-2349. We note that 200 years is not sufficient for the deep ocean to reach equilibrium, but find that model drift in the variables considered in this paper are generally very small after 200 years. The simulation labelled "REF" (Table 1) uses the same settings as the simulations in Matthes et al. (2020) with the exception that "REF", just like all our simulations, use a non-linear free-surface formulation as well as a bugfix for coupling heat fluxes when sea ice is present. The mean climate in REF is very similar to the simulations but does have an overall warmer climate. The SST is ~ 0.5 K warmer over most of the ocean and the AMOC is ~ 0.5 Sv stronger (not shown). This change is unlikely to be due to natural variability in the model since we compare 300-year averages and the warming is global.

In addition to REF, we performed six sensitivity experiments to explore the effects of atmosphere-ocean coupling time step, and lateral diffusion. In the first experiment, AHT300, the coefficient of horizontal diffusion, $A_{\mathrm{h,t}}$, is reduced from 600 $\mathrm{m}^2\ \mathrm{s}^{-1}$ to 300 $\mathrm{m}^2\ \mathrm{s}^{-1}$, similarly to Storkey et al. (2018) who also reduced diffusivity by 50%. In the two experiments CPL2H and CPL1H we alter the coupling time step between the atmosphere and ocean from the default 3 hours to 2 hours and 1 hour, respectively. Note that the lower limit of the coupling time step is the ocean model time step, 30 minutes, and that the sea-ice model time step is always the same as the coupling time step. For completeness, we also perform two additional experiments where we reduce the coefficient of horizontal diffusion as well as shorten the coupling time step, AHT300+CPL2H and AHT300+CPL1H, respectively. Finally, we perform an experiment where the sea-ice model time step and ocean-ice coupling step is reduced from 3 hours to 1 hour but the atmosphere-ocean coupling time step is kept at 3 hours, ICE1H. This experiment is only run for 300 years and we compare the last 100 years, i.e. model years 2050-2149. The ICE1H experiment is

not analysed in great detail in this paper, but will only be used to demonstrate its difference to REF and CPL1H.

All simulations start from climatological ocean temperature and salinity (Levitus et al., 1998) and an atmosphere at rest using a climatological temperature and moisture distribution. We are aware that by starting from rest our experiments are not free from model drift but as all experiments run for the same period we can isolate the impact of tunable parameters and reduce the influence of drift as best as possible in our analysis.

In addition to the coupled simulations with FOCI, we also performed two atmosphere-only experiments with ECHAM. This is to test the atmosphere model for surface wind biases over the Southern Ocean inherent to this particular component. The experiments largely follow the AMIP protocol for CMIP6, but SST and sea-ice data are taken from daily ERA-5 data (Hersbach et al., 2020). One experiment is run at the same resolution as used in FOCI, T_q63 ($\sim 1.9°$ horizontal resolution) while the other is run at T_q127 ($\sim 0.9°$), both with 95 levels as in the coupled model. Both experiments are run for the period 1979-2019, where historical forcing is used for 1979-2014 and SSP5 forcing is used for 2015-2019.

3 Results

3.1 Mean state biases in the Southern Ocean

We compare the atmosphere variables in the FOCI reference simulation to ERA-5 reanalysis (Hersbach et al., 2020), the successor of ERA-Interim which has been found to be among the most realistic reanalysis products over the Southern Ocean and Antarctica (Bromwich et al., 2011; Bracegirdle & Marshall, 2012). We also compare simulated SST as well as sea-ice concentration and area to observations from the HadISST1 dataset (Rayner, 2003). The model exhibits a substantial warm bias in Southern Ocean 2m air temperature (T2M) and SST and an underestimation of sea-ice concentration mainly in the Weddell Gyre area (Fig. 1, Table 2). The warm SST bias is present in all seasons while the T2M bias peaks in the austral winter season (JJA). The warm T2M bias overlaps with the low sea-ice bias in both location and seasonality, indicating that the T2M bias is driven by the sea-ice bias rather than the SST bias. The 10m zonal wind maximum is located too far equatorward in both DJF and JJA (Fig. 2) and the latitude of the annual-mean wind maximum is 47.6°S compared to 53.2°S in ERA-5 (Table 2). This northward shift in the westerlies appears larger in JJA compared to the other seasons.

The SST, sea ice and surface wind biases in FOCI are very similar to those in MPI-ESM-MR (Jungclaus et al., 2013) which also uses ECHAM6 at T_q63L95 resolution but has a different ocean model (MPI-OM). It was noted by Jungclaus et al. (2013) that the biases in sea-ice distribution were related to biases in sea-level pressure and thus surface winds. Hence, sea ice and surface wind biases may stem from issues inherent in the ECHAM6 atmosphere model. ECHAM6 does not suffer from the biases in cloud radiative forcing over the Southern Ocean (not shown) which is the cause of warm SST biases in many climate models in CMIP5 and CMIP6 (Hyder et al., 2018). We therefore rule out cloud biases as a source of the SST and sea-ice biases.

An atmosphere-only simulation with ECHAM6 at T_q63L95 resolution ($\sim$ 200km as used in FOCI) using daily SST and sea-ice from ERA-5 (Hersbach et al., 2020) also exhibits an equatorward bias in the westerlies, but less so than the coupled FOCI simulations (Fig. 2). The equatorward bias is reduced to a large extent when the horizontal resolution is increased to T_q127 ($\sim$ 100km) resolution. Taken together, these results imply that the equatorward bias in the atmosphere-only simulation at T_q63 is mostly due to the coarser resolution compared to T_q127. As the latitudinal position of the westerly wind maximum has been linked to surface drag (Chen et al., 2007), we speculate that the equatorward bias in ECHAM6 is due to excessive surface drag. Recent work (Savita et al., 2023) have shown a similar resolution dependence of the equatorward wind bias, albeit with a different atmosphere model. They found the resolution-dependence to stem

from the representation of shallow convection which influences the height over which surface friction acts in the atmosphere thereby controlling the momentum balance below 850 hPa. Hence, it is possible that the equatorward wind bias in ECHAM is linked to a too stratified lower atmosphere, and that increasing the horizontal resolution improves the representation of shallow convection and thus reduces the wind bias. We also note that the equatorward bias in the westerly wind maximum is larger in the coupled FOCI experiments than in the T_q63 atmosphere-only experiment. Taken together, these results indicate that the wind bias is partly inherent to the atmosphere model at this resolution but is also amplified when coupled to an ocean model. This is further discussed in Section 4.

The Drake Passage transport, a measure of ACC strength, is on average 85.6 Sv in FOCI (Table 2) which places it amongst the weakest of CMIP6-generation of models (Beadling et al., 2020) and well below the observational range of 137-173 Sv (Cunningham, 2003; Donohue et al., 2016). The Drake Passage transport has been shown to be very resolution dependent (M. J. Roberts et al., 2019) where eddy-parameterized models ($\Delta x \sim 1°$) tend to reproduce the observed strength reasonably well while increasing resolution to the eddy-present ($\Delta x \sim 0.25°$) range decreases the ACC transport significantly. In both FOCI and HadGEM-GC3 (M. J. Roberts et al., 2019), the weak ACC is caused by the presence of strong westward currents along the southern boundary of Drake Passage which are not present at coarser resolution (not shown). In experiments with HadGEM-GC3 at eddy-rich resolution ($1/12°$) the westward currents along the southern boundary are greatly reduced compared to eddy-present experiments, thus the ACC is much stronger ($\sim$ 115 Sv). We note that HadGEM-GC3 does not have a strong equatorward bias in the surface winds as FOCI does, suggesting that the wind bias may not play a role for the weak ACC, and in agreement with the non-significant relationship between wind biases and ACC biases among CMIP5 models (Beadling et al., 2019). Hence, the weak ACC in FOCI appears mostly resolution-dependent although there may also be some dependence on parameters that change with resolution as well, e.g. ACC transport has been shown to increase with increased horizontal viscosity coefficient (Megann & Storkey, 2021). The resolution dependence of the ACC is the topic of future work.

The FOCI reference simulation underestimates the Antarctic sea-ice area (SIA) by $\sim 26\%$ (Fig. 3, Table 2) with too low SIA in all seasons, particularly in the Weddell Sea area, and also a negative trend over the entire simulation. While both the Indian and Pacific sectors show biases in both SST and sea-ice concentration in JJA (Fig. 1), the largest sea-ice bias is found in the Weddell Sea where no clear SST bias exists, i.e. SST biases are not the sole explanation for the biases in Antarctic SIA. FOCI underestimates Antarctic SIA in all seasons, but more so in winter, which means that the rate of sea-ice growth in autumn is underestimated. As the autumn expansion of Antarctic SIA is controlled by surface winds to a large extent (Holland & Kwok, 2012), the Antarctic sea-ice bias in JJA may be caused by a too weak northward component in sea-ice velocities. Reduced biases in surface westerlies, i.e. stronger winds with a more poleward maximum, would likely produce stronger northward drift and increase autumn sea-ice expansion. Events of open-ocean deep convection are rare in the Southern Ocean and the occurrence of deep convection is approximately the same across all experiments (Fig. S1). We note that deep convection does not occur for the first 250 years of simulation, but then occurs in periods separated by a few decades, similarly to CMIP6 simulations from EC-Earth (same ocean model as FOCI), GFDL and MPI (same atmosphere as FOCI) (Mohrmann et al., 2021). Furthermore, while open-ocean deep convection does cause a sudden decrease in Antarctic SIA, we note that the time series of annual-mean Antarctic SIA (not shown) never reaches the observed SIA, 9.8 km^2 (Table 2). Biases in Antarctic SIA are not caused by events of open-ocean deep convection reducing the 300-year time average in REF.

3.2 Sensitivity experiments

3.2.1 Coupling time step

We find that reducing the coupling time step from 3 hours to 2 hours and 1 hour progressively cools the SST (Fig. 4) and increases the Antarctic SIA (Fig. 3, Table 2) i.e. SST and SIA biases are reduced in CPL2H and further reduced in CPL1H. A shorter coupling time step does not cause any discernible change in the zonal-mean zonal surface winds or eastward surface wind stress over the Southern Ocean in CPL2H and CPL1H (Fig. 2 and Fig. S2). One may have expected a slight increase in wind stress with shorter coupling time step through inclusion of sub-3-hourly winds, but this is not evident here. Thus, the surface wind stress over the Southern Ocean in FOCI is insensitive to the coupling time step. The reduced SST and sea-ice biases are thus not linked to any changes in 10m wind or surface wind stress.

The increased Antarctic SIA in CPL2H and CPL1H could potentially be explained by increased northward sea-ice transport which would be associated with increased sea-ice production along the Antarctic coastline and increased sea-ice melting to the north. The freshwater flux due to sea-ice formation and melting (computed by NEMO/LIM using ice-volume changes and sea-ice density 900 kg m^{-3}), F_{ice}, shows freshwater loss in the Weddell and Ross Seas and freshwater gain to the north in the reference run, consistent with ice production and brine rejection along the coastlines and melting further north (Fig. 5a). With shorter coupling time step, CPL2H and CPL1H, we find an intensification of F_{ice} compared to REF, i.e. increased ice production along the coastline and melting to the north, implying increased northward export of sea ice.

Most of the production of Antarctic sea ice occurs in coastal polynyas, where cold katabatic winds flow from the ice sheet and drive northward ice export, leaving the coastal areas ice free. The atmosphere responds with large upward turbulent heat fluxes which bring the mixed-layer temperature to the freezing point and drive the formation of frazil ice (Morales Maqueda et al., 2004; Singh et al., 2021). A shorter coupling time step allows for more frequent coupling between the atmosphere, ocean and sea-ice models; it also means a shorter time step of the sea ice model in FOCI. This is leading to slower closing of leads, a larger turbulent heat flux and enhanced sea ice export. Hence, a shorter coupling time step can cause more sea-ice production, and this is likely the mechanism by which biases in SST and SIA are reduced in CPL2H and CPL1H. We note that the closing of leads also depends on the thickness of newly formed ice which is controlled by a parameter, `hiccrit`, set to 0.6 m in all our experiments. Since the prognostic variable is ice volume, a lower value would cause leads to close faster and newly formed ice to be thinner.

The ICE1H experiment, where the LIM2 time step as well as the ocean-ice coupling time step (between NEMO and LIM2) is shortened to 1 hour while the OASIS coupling step is kept at 3 hour, does not exhibit any of the reductions in surface biases as found in CPL1H. The Antarctic sea-ice concentration is considerably lower in ICE1H compared to the reference experiment (Fig. 6), and the SST is higher (not shown). As the atmospheric turbulent heat fluxes are only updated every 3 hours in ICE1H the atmosphere is not always "aware" of a newly formed coastal polynya. The turbulent heat flux response to the opening of a coastal polynya is reduced which inhibits frazil ice formation. Hence, the increased Antarctic SIA in CPL1H and AHT300+CPL1H is likely due to a combination of both the shorter OASIS coupling time step as well as the shorter LIM2 time step.

The surface freshwater flux changes associated with a larger Antarctic sea-ice cover in runs with shorter coupling time step strongly reduce the fresh bias on the shelf and locally weakens the salinity gradient (Fig. 7). In the Weddell Sea, the increased F_{ice} in CPL1H and CPL2H compared to REF act to reduce the salinity gradient on the shelf as well as on the northern edge of the Weddell Gyre, and the Weddell Gyre weakens as a result (Table 2, Fig. S3). While we do not find any discernible change in surface wind stress from the atmosphere (Fig. S2), it is possible that the increased sea-ice cover in

CPL2H and CPL1H compared to REF means a less rough surface and thus reducing the momentum transfer to the ocean and possibly also acting to weaken the Weddell Gyre. The weakening of the Weddell Gyre reduces the poleward heat transport (Table 2, Fig S4) by 0.02 PW and 0.04 PW in CPL2H and CPL1H respectively which causes a cooling at the surface as well as down to depths of $\sim$ 4000 m (Fig. 8).

Weddell Sea cross sections of salinity and temperature in CPL2H and CPL1H (Figs. S5,S6) show that the changes at depth largely occur along iso-pycnals. It is likely that the cooling and freshening below 500m is due to the weakening of the Weddell and Ross Gyres which reduces the advection of warm and salty water from lower latitudes towards Antarctica, as also indicated by the reduction of poleward heat transport (Table 2).

While the Weddell Gyre weakens in CPL1H and CPL2H, the increased F_{ice} also causes a stronger zonal-mean meridional density gradient which likely explains the slight strengthening of the Drake Passage transport, in agreement with the positive correlation between meridional density gradients and Drake Passage transports in CMIP5 models (Beadling et al., 2019).

It may be possible to weaken the Weddell Gyre and thus achieve a similar reduction in poleward heat transport as in CPL1H by increasing the eddy-induced tracer diffusion from the GM scheme. However, we note that the magnitude of eddy-induced tracer diffusion in all our experiments never reaches the already set upper limit of 1000 $\mathrm{m^2\ s^{-1}}$. Hence, our chosen upper limit has no impact on the Weddell Gyre strength or the ocean circulation in the Southern Ocean overall.

The CPL2H and CPL1H simulations also exhibit enhanced sea-ice freshwater flux, F_{ice} in the Arctic compared to REF (not shown), i.e. more ice production in the central Arctic and more melting along the sea-ice edge. The increased F_{ice} could be caused by a stronger heat flux response to opening leads in the sea-ice pack, similarly to the increased F_{ice} in the Antarctic coastal polynyas.

3.2.2 Iso-neutral diffusion

Reducing the horizontal diffusion coefficient, $A_{\mathrm{h,t}}$ from 600 $\mathrm{m^2\ s^{-1}}$ to 300 $\mathrm{m^2\ s^{-1}}$ leads to a slight decrease of the Southern Ocean SST but has a relatively small impact on the surface biases in FOCI compared to changing the coupling time step. The SST cools by $\sim$ 0.5K upstream of Drake Passage in AHT300 compared to the reference experiment (Fig. 4) and the sea-ice cover is larger (Table 2) and thus closer to observations. We found the impact of changing $A_{\mathrm{h,t}}$ to be rather independent of the coupling time step for all quantities discussed and thus refrain from presenting additional difference maps isolating such response for the CPL2H and CPL1H cases. While the surface is colder, the water masses at $\sim$ 2000m depth, likely CDW, are warmer and saltier which, as suggested by Hieronymus and Nycander (2013) and Storkey et al. (2018), may be due to reduced upward transport of heat and salt which would also explain the surface cooling and freshening at the surface. The cooling of SST in AHT300 primarily happens around the Drake Passage, i.e. not where the most prominent warm SST bias exists in the reference experiment. Hence, AHT300 improves the zonal mean SST mostly by compensation of errors.

The AHT300 experiment shows a weakening of the Atlantic Meridional Overturning Circulation (AMOC) compared to REF (Table 2). This is an improvement as the reference experiment has an AMOC that is slightly stronger than observed by the RAPID array (16.9 Sv) (Moat et al., 2022; Matthes et al., 2020). We also find that AHT300 has a colder subpolar North Atlantic (Fig. S7) than REF, which increases the existing cold bias in REF. As iso-neutral diffusion is a large part of the surface heat budgets in both the Southern Ocean and subpolar North Atlantic (Hieronymus & Nycander, 2013) by transporting heat upward, the increased cold bias in AHT300 is likely not due to the weaker AMOC but rather the weaker mixing.

The AHT300 simulation shows a distinct spin-up of the Weddell Gyre by 2.3 Sv and an increased poleward heat transport of 0.2 PW, in contradiction to the weaker gyre

and reduced heat transport in CPL2H and CPL1H. The Weddell Gyre strength in FOCI, 82.2 Sv is clearly above the observational estimates of $\sim$ 50 Sv (Klatt et al., 2005), so a further increase exacerbates the model bias of gyre strength and likely also for poleward heat transport (S4). The stronger Weddell Gyre in AHT300 is likely due to steeper isopycnals as a result of the weaker horizontal diffusion.

The global meridional overturning circulation in REF shows the upper-ocean Sub-Tropical Cells (STC), the Deacon Cell in the Southern Ocean and the AMOC (Fig. 9a). A lower cell where Antarctic Bottom Water (AABW) is carried from the Southern Ocean northward into the other basins is very weak and not well visible. The overturning circulation is very similar to that of the *KIEL* ocean-sea ice model in Farneti et al. (2015) which used the same grid as FOCI but an older version of NEMO. Reducing the coupling time step in CPL2H and CPL1H results in a more vigorous overturning in the Southern Ocean (Fig. 9b-c) where both the Deacon Cell around 50°S and the lower (AABW) cell strengthen, suggesting more deep-water formation. The lower AABW cell intensification is found between 50S and 20N, indicating more northward AABW transport. In contrast, reducing tracer diffusion in AHT300 results in a weakening of the AMOC in the North Atlantic (Fig. 9d) with no apparent change in the lower AABW cell.

The meridional overturning computed in potential density classes, σ_2 (referenced to 2000m) further reveals water-mass transformations of the meridional overturning by filtering out iso-pycnal motions. The REF experiment shows the STC and AMOC, along with a clockwise (positive) Southern Ocean cell producing Antarctic Intermediate Water, an anti-clockwise subpolar cell arising partly from the Weddell and Ross Gyres, and a weak anti-clockwise lower cell at higher densities than the AMOC representing the AABW (Fig. 10a). As was the case for the circulation in depth coordinates, REF is very similar to *KIEL* of Farneti et al. (2015). The CPL2H and CPL1H show an intensification of the AABW cell as well as a shift toward denser water masses in the subpolar cell (Fig. 10b,c), evincing the increased formation of AABW. The stronger AABW cell and increased AABW formation is likely due to the increased sea-ice production and increased brine rejection along the Antarctic coast (Fig. 5) driving more downward transport of cold, salty water. Both CPL2H and CPL1H also show an intensification of the AMOC around $\sigma_2 \sim 36.85$ kg m^{-3} which could be due to the North Atlantic Deep Water becoming denser.

Similarly to CPL2H and CPL1H, AHT300 shows an intensification of the lower AABW cell (Fig. 10d), albeit with no change in the subpolar cell, indicating a stronger AABW cell between $\sim$ 40°S and $\sim$ 30°N but no change in AABW formation. The stronger AABW cell, as well as the shift of AMOC to higher density in the North Atlantic (Fig. 10d) could be due to less water-mass transformation from diffusion so that the deep water formed in the North Atlantic and Southern Ocean retains its properties for longer before mixing with other water masses.

3.2.3 Combined effects

When combining both reduced horizontal diffusion and reduced coupling time steps, AHT300+CPL2H and AHT300+CPL1H, we find the changes in zonal-mean temperature and salinity in both simulations to be approximately linear combinations of AHT300 and CPL2H and CPL1H, respectively. The response of the zonal-mean temperature and salinity (Fig. 8, 7) as well as SST (Fig. 4) are nearly as one would expect by adding AHT300 to CPL2H and AHT300 to CPL1H. However, we also observe non-linearities in the response of Antarctic SIA (Fig. 3) and the meridional overturning circulation (Fig. 9), which is to be expected as the two are linked via sea-ice production and AABW production. The increase in annual-mean Antarctic SIA in AHT300, CPL2H, and CPL1H are $0.8 \cdot 10^6$ km^2, $1.8 \cdot 10^6$ km^2, and $2.2 \cdot 10^6$ km^2, respectively, while for AHT300+CPL2H and AHT300+CPL1H it is $2.5 \cdot 10^6$ km^2 and $2.7 \cdot 10^6$ km^2 respectively. The responses are thus not linear combinations of AHT300 with CPL2H and CPL1H. We speculate that the various strategies for increasing the Antarctic SIA likely has diminishing returns as

the sea ice expands further north and encounters warmer water. Likewise, the response in Drake Passage transport is non-linear, where AHT300 results in a weaker transport while it strengthens in CPL2H and CPL1H, and there is a further strengthening in AHT300+CPL1H. It is also possible that some of the deviations from linear responses can be due to modes of multi-centennial variability in the Southern Ocean which have been observed in climate models (Park & Latif, 2008).

The changes in SST following a shorter coupling step in CPL2H and CPL1H are mostly confined to the Southern Ocean, although a cooling of SSTs are also found in the subpolar North Atlantic Ocean and in particular the Barents Sea (Supplementary Material, Fig. 2). The cooling may be explained by a reduction in the poleward oceanic heat transport in the Atlantic at 45°N of ~ 0.01 PW or $\sim 2\%$ in CPL1H, CPL2H, AHT300+CPL1H, AHT300+CPL2H (SM9). However, we note that the poleward heat transport increases in AHT300 by a similar magnitude and also that the cooling in AHT300 is larger than in CPL2H, CPL1H. It is thus likely that most of the surface cooling in the North Atlantic in AHT300+CPL2H and AHT300+CPL1H is due to the reduced iso-neutral diffusion causing less heat to reach the surface. We also note that AMOC weakens in all sensitivity experiments compared to REF and that the weakened AMOC is an improvement compared to REF which had a too strong AMOC.

4 Discussion & Conclusions

We have explored a number of ways to mitigate climate biases in the Southern Ocean both at the surface and at depth in the FOCI coupled climate model. We found that shortening the coupling time step from 3 hours to 1 hour reduced biases in SST and Antarctic SIA, while the ACC strength bias was only slightly improved, and wind biases were hardly affected at all. The biases in temperature and salinity were also reduced throughout the upper 3000 m, with the largest reduction found at 1000 m depth. We propose that the shorter coupling time step between the atmosphere, ocean and sea-ice models caused stronger response of turbulent heat fluxes and ice advection in coastal polynyas, thereby increasing sea-ice production and overall Antarctic SIA. The increased sea-ice production caused more water-mass transformations in coastal polynyas and more formation of AABW, as indicated by the intensification of the AABW overturning cell. Reducing the coupling time step also lead to a weaker Weddell Gyre and overall reduced poleward heat transport, thus reducing temperature and salinity biases at depth.

Reducing the coupling time step in FOCI in e.g. CPL1H and CPL1H+AHT300 experiments was accompanied by a reduction of the time step of the sea-ice model call, which is generally synchronized with the atmosphere-ocean coupling. An experiment ICE1H with 1 hour sea-ice model time step and 3 hour coupling time step did not show the reduction in biases found in CPL1H (Fig. S8). The results imply that the improvements in CPL2H and CPL1H are due to reducing both the sea-ice model time step and coupling time step simultaneously, so that the atmosphere model can produce a heat flux response to sea-ice anomalies in coastal polynyas and enhance sea-ice production.

Reducing the coefficient for iso-neutral tracer diffusion had a comparatively small effect, as demonstrated by the CPL1H and CPL1H+AHT300 simulations exhibiting very similar mean states. Excessive iso-neutral diffusion was noted to cause a warm SST bias in the Southern Ocean in the MetOffice GO6 and HadGEM-MM simulations, likely by enhancing upward heat transport (Storkey et al., 2018). Our results suggest that excessive upward heat transport by iso-neutral diffusion was not the main cause of the SST bias in the FOCI reference experiment.

Overall, our sensitivity experiments showed only small changes to the simulated ocean circulation and climate outside the Southern Ocean compared to the reference experiment. In particular we note that shortening the coupling time step lead to increased sea-ice production and better representation of observed sea ice and SST in the Southern Ocean without any large changes in the Arctic. Reduced iso-neutral diffusion caused a decrease of the SST in the North Atlantic subpolar seas and a weakening of the sub-

polar gyre (Fig. S3) likely due to the reduced upward heat transport by iso-neutral diffusion (Hieronymus & Nycander, 2013).

It is clear from all sensitivity experiments that the equatorward bias in the westerly wind maximum is insensitive to the underlying biases in SST and sea-ice extent. An AMIP run at T_q127 resolution ($\sim$ 100km) exhibits a smaller bias than T_q63 ($\sim$ 200km), indicating that the bias is resolution-dependent, while the fact that AMIP experiments show a smaller bias than the coupled experiments suggests that the bias is amplified in coupled mode. We stress that the AMIP experiments and ERA-5 both represent present-day conditions while the FOCI experiments represent pre-industrial conditions and that the difference in jet stream position could partly be due the anthropogenic forcing since 1850. Coupled models in CMIP5 showed an approximately $\sim 1^\circ$ poleward shift in the Southern Hemisphere jet stream position from pre-industrial (*piControl*) and present-day (*historical*) simulations and a further $\sim 2^\circ$ shift in 2100 under a high-emission scenario (*RCP8.5*) (Barnes & Polvani, 2013). The wind maximum in FOCI is $\sim 5^\circ$ equatorward of that in ERA-5. It is thus very unlikely that the wind maximum latitude bias in FOCI is due to the fact that all runs are pre-industrial control runs.

Previous studies have shown that the latitude of the westerly wind maximum is sensitive to the magnitude of surface friction (Chen et al., 2007), with stronger friction causing weaker and more equatorward winds as found in our experiments. A possible mechanism in FOCI could be that the marine boundary layer is too shallow, causing friction to have a strong effect in the boundary layer. Increasing boundary-layer mixing could be a way to increase vertical mixing of momentum in the lower troposphere, distributing the effect of friction over a larger depth, and thus accelerating the surface winds and pushing the wind maximum poleward. Such a mechanism was recently found in the OpenIFS atmosphere model (Savita et al., 2023). However, we also note that Ayres et al. (2022) found a weakening and equatorward shift of the tropospheric jet in an experiment with a large reduction of Antarctic sea ice, suggesting that a large negative sea-ice bias may cause an equatorward bias in the westerly jet maximum. It is possible that the reduction in sea-ice bias in our sensitivity experiments are not large enough to shift the jet.

Using a shorter coupling time step in FOCI is computationally prohibitive since it increases communication between the atmosphere and ocean model at runtime which leads to an overall slower model. Indeed, we find that CPL1H is $15-20\%$ slower than the default piControl simulation. The slowdown with shorter coupling time step also comes from poor synchronisation with the radiation scheme in ECHAM which is called every two hours. Despite the slower model, we argue that 1hr coupling time step is preferable over 2 or 3 hours.

The results in this paper suggest that coupled models should aim for a coupling time step of no more than 1 hour and that the coefficient for iso-neutral tracer diffusion should be chosen with care. We do not recommend reducing the coefficient $A_{\mathrm{h,t}}$ in our configuration, but note that Storkey et al. (2018) found improvement following a 50% reduction albeit with higher horizontal and vertical resolution. The reduced surface biases in CPL1H and CPL1H+AHT300 compared to the reference simulation will be important for future model simulations with ocean biogeochemistry as many biogeochemical processes are dependent on the SST and seasonal sea-ice cycle. Furthermore, the intensification of the AABW cell in CPL1H suggests that reducing the coupling time step may increase oceanic carbon uptake.

Open Research Section

Data Availability Statement

This study made use of output from the FOCI climate model as well as ERA-5 reanalysis (Hersbach et al., 2023, 2023), SST and sea-ice data from HadISST1 (Rayner, 2003), and ocean temperature and salinity data from WOA98 (Levitus et al., 1998). Source code needed to reproduce model experiments, Jupyter notebooks to reproduce all fig-

ures, and processed data (time averages etc.) can be found at `https://doi.org/10.5281/zenodo.8305165`. The full model output is available from the corresponding author upon reasonable request. The FOCI source code is identical to that used in Matthes et al. (2020) and is available under license from MPI-M Hamburg (ECHAM6), IPSL Paris (NEMO/LIM) and CERFACS Toulouse (OASIS) and is under LGPL or Cecill License.

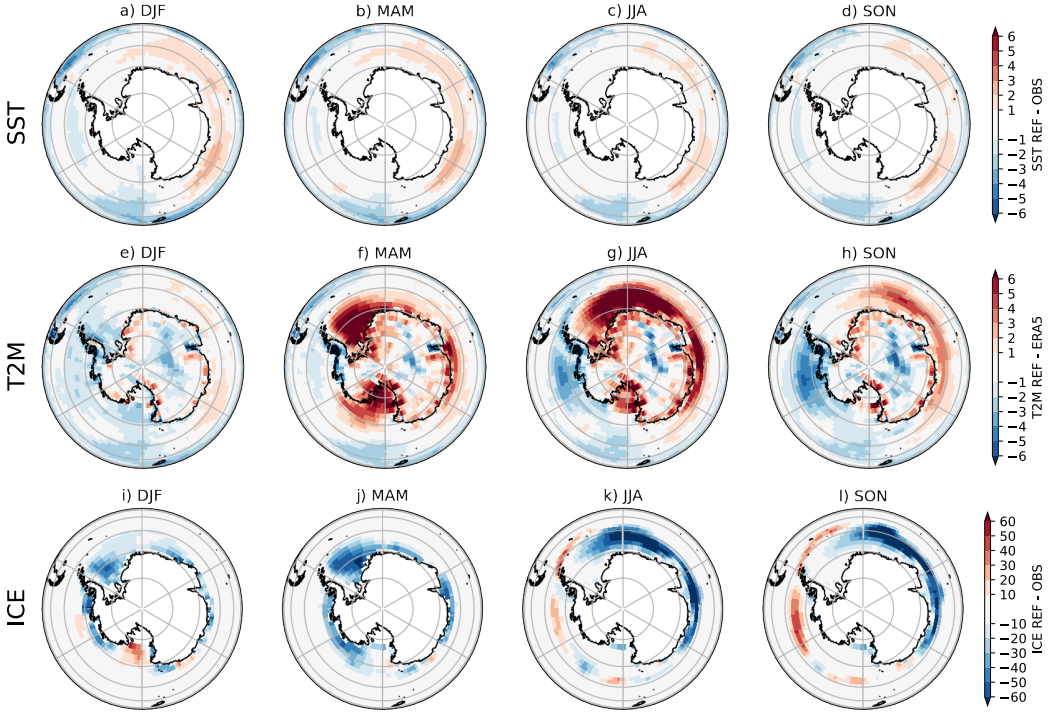

Figure 1. Seasonal biases in SST (a-d), 2m air temperature (e-h) and sea-ice concentration (i-l) in the REF pre-industrial control simulation.

Acknowledgments

The FOCI simulations were carried out at the HLRN-IV supercomputer and all analysis was conducted on the NESH cluster at CAU, Kiel. JK acknowledges support from JPI Climate & JPI Oceans (ROADMAP, grant 01LP2002C). MÖ acknowledges support from EU Horizon 2020 (SO-CHIC, grant 821001). MZ and TM were supported by the German Federal Ministry of Education and Research (BMBF) as a Research for Sustainability initiative (FONA) through the project PalMod: From the Last Interglacial to the Anthropocene – Modeling a Complete Glacial Cycle (FKZ: 01LP1918C).

The authors declare no conflicts of interest.

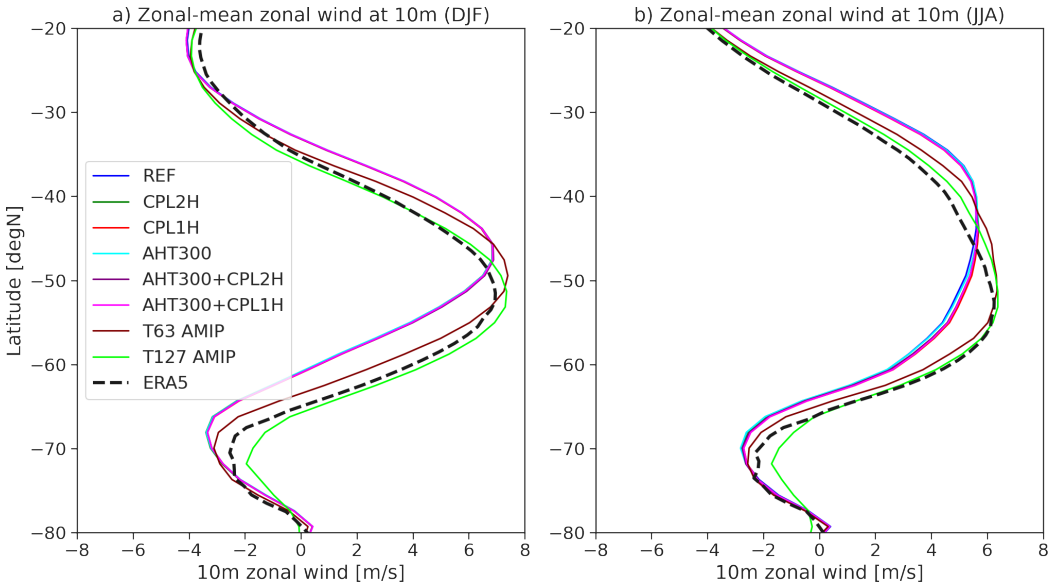

Figure 2. Zonal-mean zonal wind at 10m height for all simulations (coloured lines) and ERA-5 reanalysis (black dashed line) for summer (DJF, a) and winter (JJA, b).

Table 1. Model runs used in this paper. See Data section of paper for details. All runs start from an ocean at rest, ocean potential temperature and salinity initialized from the WOA98 climatology (Levitus et al., 1998) and under constant pi-control climate conditions. NLFS refers to non-linear free surface formulation with variable volume layer (vvl) in NEMO.

Name	ID	Simulation Time	Note
REF	SW087	1850-2371	as FOCI-piCtl of Matthes et al. (2020) but with NLFS
CPL2H	SW106	1850-2349	as REF, but coupling frequency 2 hours
CPL1H	SW098	1850-2349	as REF, but coupling frequency 1 hour
ICE1H	SW202	1850-2149	as REF, but ocean-ice coupling step 1 hour
AHT300	SW082	1850-2350	as REF, but horiz. tracer diffusion halved to 300 m^2 s^{-1}
AHT300+CPL2H	SW120	1850-2378	CPL2H and AHT300 combined
AHT300+CPL1H	SW111	1850-2499	CPL1H and AHT300 combined
ECHAM-T63	SH007	1979-2019	Atmosphere-only with daily ERA-5 SST/sea ice
ECHAM-T127	RP002	1979-2019	Atmosphere-only with daily ERA-5 SST/sea ice

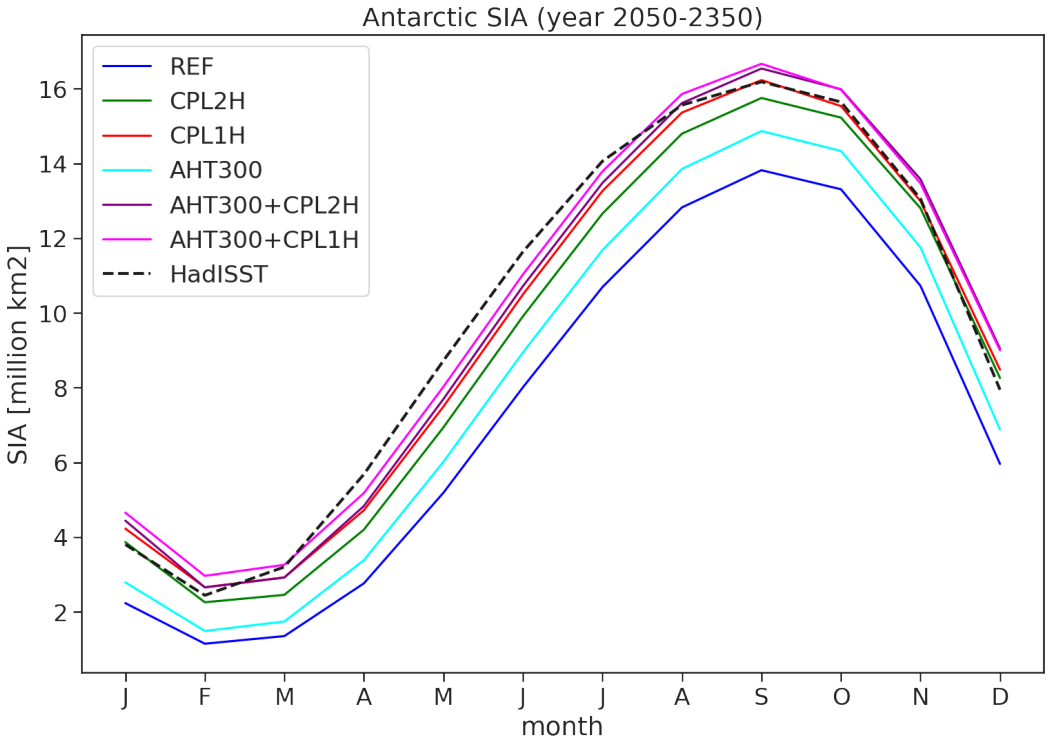

Figure 3. Mean seasonal cycle of Antarctic SIA in all experiments averaged over the years 2050-2350. Black dashed line corresponds to observations from HadISST for 1979-2020.

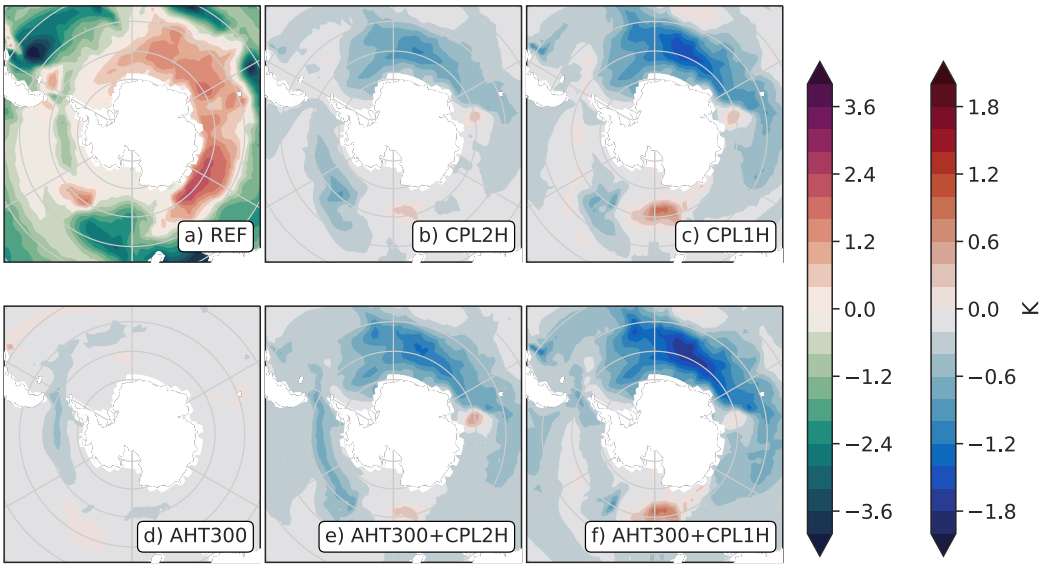

Figure 4. a) Time mean (year 200-500) SST bias in REF compared to HadISST 1979-2020. b-f) Difference between each experiment and REF. The left colorbar belongs to Fig. a. The right colorbar belongs to panels b-f.

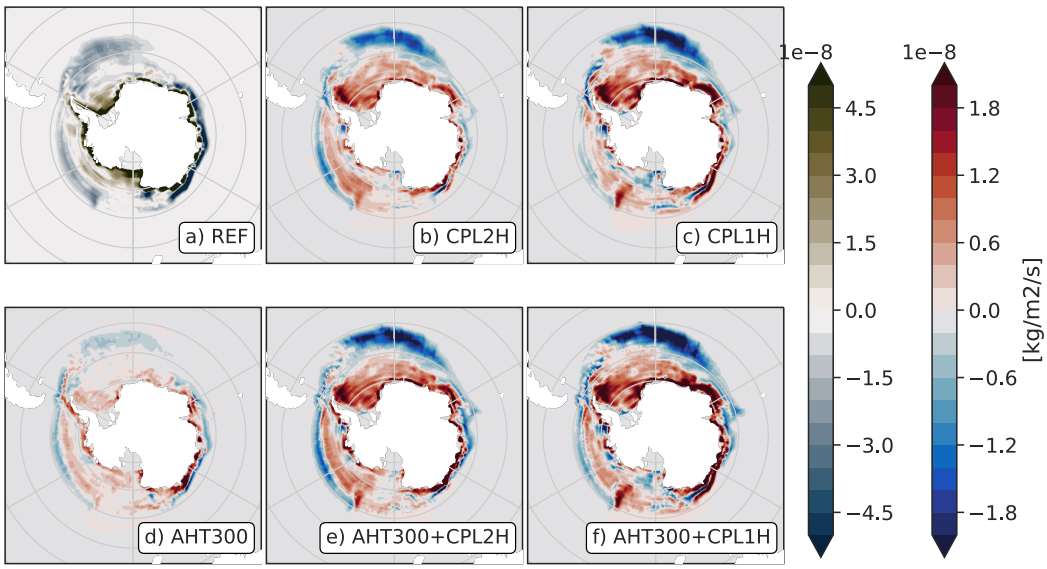

Figure 5. a) Time mean (year 200-500) freshwater flux due to sea ice freezing/melting in REF. b-f) Difference between each experiment and REF. The left colorbar belongs to Fig. a. The right colorbar belongs to panels b-f.

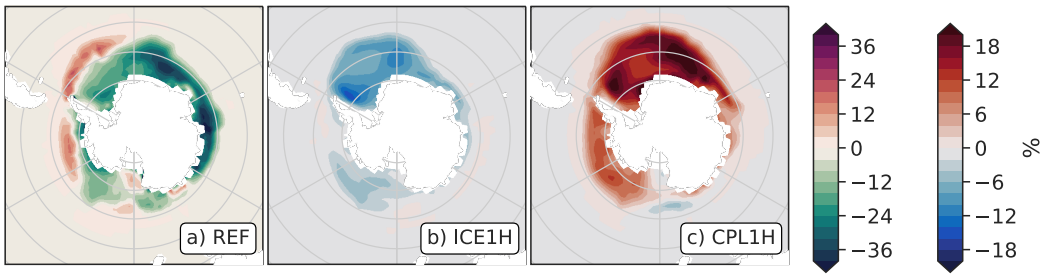

Figure 6. Annual-mean sea-ice concentration bias (compared to HadISST 1979-2020) in a) REF, b) ICE1H and c) CPL1H experiments. Panel a is the average of Fig. 1a-d. The left colorbar belongs to Fig. a. The right colorbar belongs to Figs. b,c.

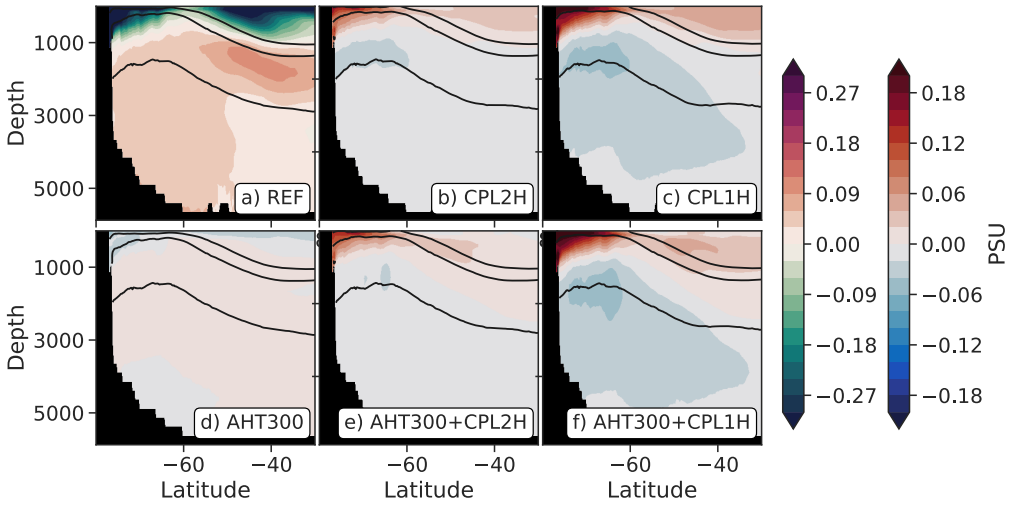

Figure 7. a) Time mean (year 200-500) zonal-mean salinity bias with respect to WOA98 (Levitus et al., 1998) climatology. b-f) Difference between each experiment and REF. Solid black contours are drawn for $\sigma_0 = 27.2, 27.5, 27.8$ kg m^{-3} in each experiment. The left colorbar belongs to Fig. a. The right colorbar belongs to Figs. b-f.

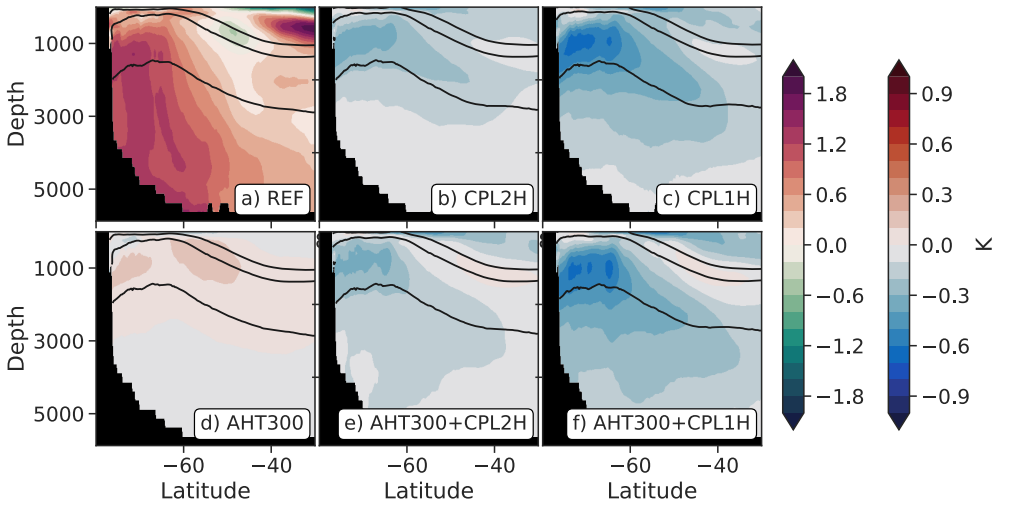

Figure 8. As Fig. 7 but for potential temperature.

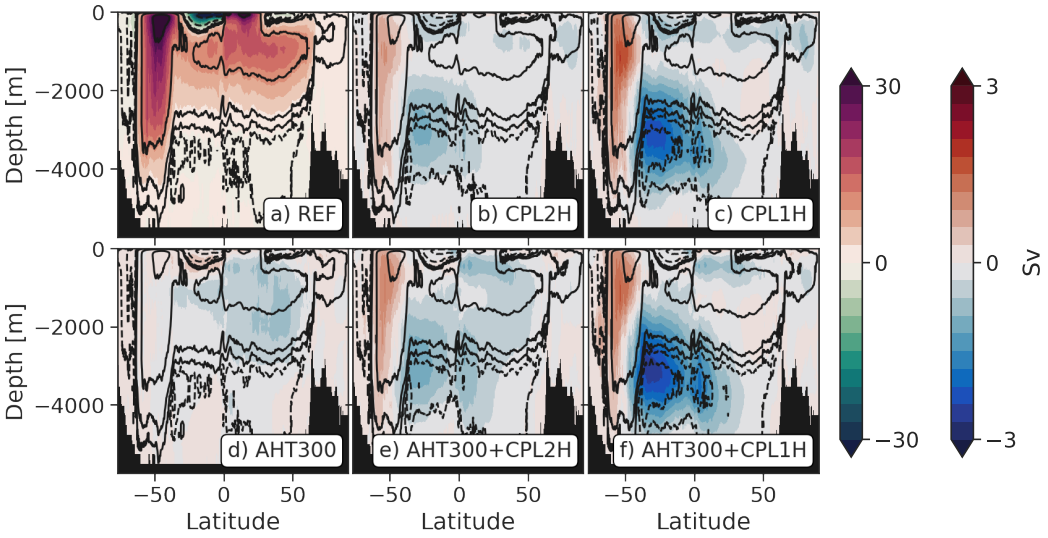

Figure 9. Time mean global meridional overturning stream functions in REF (a) and difference to REF for all other experiments (b-f). The left colorbar belongs to Fig. a. The right colorbar belongs to Figs. b-f.

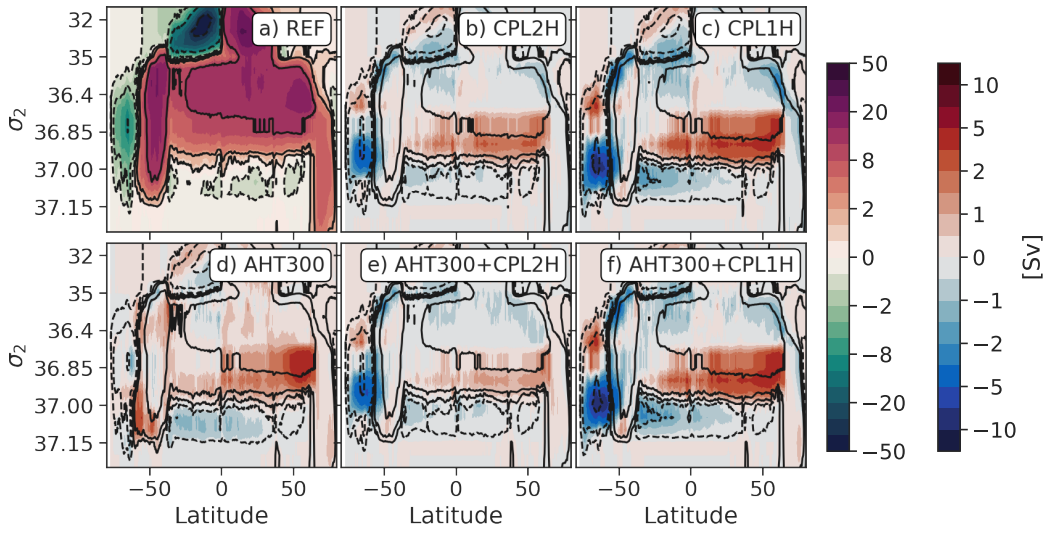

Figure 10. As Fig. 9 but in (y, σ_2) coordinates.

Table 2. Performance metrics for all simulations. All data are annual means. Sea-ice data is taken from HadISST (Rayner, 2003), AMOC data from RAPID (Moat et al., 2022), Weddell Gyre strength from Klatt et al. (2005), Drake Passage transport estimates are from Cunningham (2003) and Donohue et al. (2016), wind data from ERA-5 (Hersbach et al., 2020).

	Ref.	AHT300	CPL2H	CPL1H	CPL2H+AHT300	CPL1H+AHT300	Obs.
Arctic SIA [km^2]	10.2	10.3	10.6	10.8	10.7	10.8	10.4
Antarctic SIA [km^2]	7.3	8.1	9.1	9.5	9.8	10.0	9.8
AMOC, 26.5°N [Sv]	17.6	16.9	17.3	17.2	17.0	17.1	16.9
Wedd. Gyre [Sv]	82.2	84.5	77.9	72.3	80.0	72.3	56
Drake Pass. [Sv]	85.6	84.8	86.6	90.7	87.2	92.0	$137 - 173$
Wind maximum [°S]	47.6	47.6	47.6	47.6	47.6	47.6	52.5
Heat trans, 70°S [PW]	−0.20	−0.22	−0.18	−0.16	−0.18	−0.15	

References

Ayres, H. C., Screen, J. A., Blockley, E. W., & Bracegirdle, T. J. (2022, 7). The Coupled Atmosphere–Ocean Response to Antarctic Sea Ice Loss. *Journal of Climate*, *35*(14), 4665–4685. Retrieved from https://journals.ametsoc.org/view/journals/clim/35/14/JCLI-D-21-0918.1.xml doi: 10.1175/JCLI-D-21-0918.1

Barnes, E. A., & Polvani, L. (2013). Response of the midlatitude jets, and of their variability, to increased greenhouse gases in the CMIP5 models. *Journal of Climate*, *26*(18), 7117–7135. doi: 10.1175/JCLI-D-12-00536.1

Beadling, R. L., Russell, J. L., Stouffer, R. J., Goodman, P. J., & Mazloff, M. (2019, 9). Assessing the Quality of Southern Ocean Circulation in CMIP5 AOGCM and Earth System Model Simulations. *Journal of Climate*, *32*(18), 5915–5940. Retrieved from http://journals.ametsoc.org/doi/10.1175/JCLI-D-19-0263.1 doi: 10.1175/JCLI-D-19-0263.1

Beadling, R. L., Russell, J. L., Stouffer, R. J., Mazloff, M., Talley, L. D., Goodman, P. J., ... Pandde, A. (2020). Representation of Southern Ocean Properties across Coupled Model Intercomparison Project Generations: CMIP3 to CMIP6. *Journal of Climate*, *33*(15), 6555–6581. doi: 10.1175/JCLI-D-19-0970.1

Boucher, O., Servonnat, J., Albright, A. L., Aumont, O., Balkanski, Y., Bastrikov, V., ... Vuichard, N. (2020). Presentation and Evaluation of the IPSL-CM6A-LR Climate Model. *Journal of Advances in Modeling Earth Systems*, *12*(7), 1–52. doi: 10.1029/2019MS002010

Bracegirdle, T. J., Holmes, C. R., Hosking, J. S., Marshall, G. J., Osman, M., Patterson, M., & Rackow, T. (2020, 6). Improvements in Circumpolar Southern Hemisphere Extratropical Atmospheric Circulation in CMIP6 Compared to CMIP5. *Earth and Space Science*, *7*(6), 1–12. Retrieved from https://onlinelibrary.wiley.com/doi/abs/10.1029/2019EA001065 doi: 10.1029/2019EA001065

Bracegirdle, T. J., & Marshall, G. J. (2012). The reliability of Antarctic tropospheric pressure and temperature in the latest global reanalyses. *J. Clim.*, *25*, 7138–7146.

Bracegirdle, T. J., Shuckburgh, E., Sallee, J. B., Wang, Z., Meijers, A. J., Bruneau, N., ... Wilcox, L. J. (2013). Assessment of surface winds over the atlantic, indian, and pacific ocean sectors of the southern ocean in cmip5 models: Historical bias, forcing response, and state dependence. *Journal of Geophysical Research Atmospheres*, *118*(2), 547–562. doi: 10.1002/jgrd.50153

Bromwich, D. H., Nicolas, J. P., & Monaghan, A. J. (2011, 8). An Assessment of Precipitation Changes over Antarctica and the Southern Ocean since 1989 in Contemporary Global Reanalyses*. *Journal of Climate*, *24*(16), 4189–4209. Retrieved from http://journals.ametsoc.org/doi/10.1175/2011JCLI4074.1 doi: 10.1175/2011JCLI4074.1

Calvert, D., & Siddorn, J. (2013). Revised vertical mixing parameters for the UK community standard configuration of the global NEMO ocean model. *Hadley Centre Technical Note 95*.

Chen, G., Held, I. M., & Robinson, W. A. (2007, 8). Sensitivity of the Latitude of the Surface Westerlies to Surface Friction. *Journal of the Atmospheric Sciences*, *64*(8), 2899–2915. Retrieved from https://journals.ametsoc.org/doi/10.1175/JAS3995.1 doi: 10.1175/JAS3995.1

Craig, A., Valcke, S., & Coquart, L. (2017, 9). Development and performance of a new version of the OASIS coupler, OASIS3-MCT_3.0. *Geoscientific Model Development*, *10*(9), 3297–3308. Retrieved from https://www.geosci-model-dev.net/10/3297/2017/ doi: 10.5194/gmd-10-3297-2017

Cunningham, S. A. (2003). Transport and variability of the Antarctic Circumpolar Current in Drake Passage. *Journal of Geophysical Research*, *108*(C5),

8084. Retrieved from http://doi.wiley.com/10.1029/2001JC001147 doi: 10.1029/2001JC001147

Donohue, K. A., Tracey, K. L., Watts, D. R., Chidichimo, M. P., & Chereskin, T. K. (2016). Mean Antarctic Circumpolar Current transport measured in Drake Passage. *Geophysical Research Letters*, *43*(22), 760–11. doi: 10.1002/2016GL070319

Döös, K. (1995). Interocean exchange of water masses. *Journal of Geophysical Research*, *100*(C7), 13499–13514.

Döscher, R., Acosta, M., Alessandri, A., Anthoni, P., Arsouze, T., Bergman, T., ... Zhang, Q. (2022, 4). The EC-Earth3 Earth system model for the Coupled Model Intercomparison Project 6. *Geoscientific Model Development*, *15*(7), 2973–3020. Retrieved from https://gmd.copernicus.org/articles/15/2973/2022/ doi: 10.5194/gmd-15-2973-2022

Farneti, R., Downes, S. M., Griffies, S. M., Marsland, S. J., Behrens, E., Bentsen, M., ... Yeager, S. G. (2015, 9). An assessment of Antarctic Circumpolar Current and Southern Ocean meridional overturning circulation during 1958–2007 in a suite of interannual CORE-II simulations. *Ocean Modelling*, *93*, 84–120. Retrieved from https://linkinghub.elsevier.com/retrieve/pii/S1463500315001183 doi: 10.1016/j.ocemod.2015.07.009

Fichefet, T., & Maqueda, M. A. M. (1997, 6). Sensitivity of a global sea ice model to the treatment of ice thermodynamics and dynamics. *Journal of Geophysical Research: Oceans*, *102*(C6), 12609–12646. Retrieved from http://doi.wiley.com/10.1029/97JC00480 doi: 10.1029/97JC00480

Frölicher, T. L., Sarmiento, J. L., Paynter, D. J., Dunne, J. P., Krasting, J. P., & Winton, M. (2015, 1). Dominance of the Southern Ocean in Anthropogenic Carbon and Heat Uptake in CMIP5 Models. *Journal of Climate*, *28*(2), 862–886. Retrieved from http://journals.ametsoc.org/doi/10.1175/JCLI-D-14-00117.1 doi: 10.1175/JCLI-D-14-00117.1

Gent, P. R., & McWilliams, J. C. (1990). Isopycnal mixing in ocean circulation models. *J. Phys. Oceanogr.*, *20*, 150–155.

Hersbach, H., Bell, B., Berrisford, P., Biavati, G., Horányi, A., Muñoz Sabater, J., ... Thépaut, J.-N. (2023). *ERA5 monthly averaged data on single levels from 1940 to present* (Tech. Rep.). Copernicus Climate Change Service (C3S) Climate Data Store (CDS). doi: 10.24381/cds.f17050d7

Hersbach, H., Bell, B., Berrisford, P., Hirahara, S., Horányi, A., Muñoz-Sabater, J., ... Thépaut, J. (2020, 6). The ERA5 global reanalysis. *Quarterly Journal of the Royal Meteorological Society*(September 2019), qj.3803. Retrieved from https://onlinelibrary.wiley.com/doi/abs/10.1002/qj.3803 doi: 10.1002/qj.3803

Heuzé, C. (2021, 1). Antarctic Bottom Water and North Atlantic Deep Water in CMIP6 models. *Ocean Science*, *17*(1), 59–90. Retrieved from https://os.copernicus.org/articles/17/59/2021/ doi: 10.5194/os-17-59-2021

Heuzé, C., Heywood, K. J., Stevens, D. P., & Ridley, J. K. (2013, 4). Southern Ocean bottom water characteristics in CMIP5 models. *Geophysical Research Letters*, *40*(7), 1409–1414. Retrieved from http://doi.wiley.com/10.1002/grl.50287 doi: 10.1002/grl.50287

Hewitt, H. T., Roberts, M. J., Hyder, P., Graham, T., Rae, J., Belcher, S. E., ... Wood, R. A. (2016, 10). The impact of resolving the Rossby radius at mid-latitudes in the ocean: results from a high-resolution version of the Met Office GC2 coupled model. *Geoscientific Model Development*, *9*(10), 3655–3670. Retrieved from https://www.geosci-model-dev.net/9/3655/2016/ doi: 10.5194/gmd-9-3655-2016

Hieronymus, M., & Nycander, J. (2013, 7). The budgets of heat and salinity in NEMO. *Ocean Modelling*, *67*, 28–38. Retrieved from https://linkinghub.elsevier.com/retrieve/pii/S1463500313000462 doi: 10.1016/j.ocemod

.2013.03.006

Holland, P. R., & Kwok, R. (2012, 12). Wind-driven trends in Antarctic sea-ice drift. *Nature Geoscience*, *5*(12), 872–875. Retrieved from http://www.nature.com/articles/ngeo1627 doi: 10.1038/ngeo1627

Hyder, P., Edwards, J. M., Allan, R. P., Hewitt, H. T., Bracegirdle, T. J., Gregory, J. M., ... Belcher, S. E. (2018). Critical Southern Ocean climate model biases traced to atmospheric model cloud errors. *Nature Communications*, *9*(1). Retrieved from http://dx.doi.org/10.1038/s41467-018-05634-2 doi: 10.1038/s41467-018-05634-2

Jungclaus, J. H., Fischer, N., Haak, H., Lohmann, K., Marotzke, J., Matei, D., ... Von Storch, J. S. (2013). Characteristics of the ocean simulations in the Max Planck Institute Ocean Model (MPIOM) the ocean component of the MPI-Earth system model. *Journal of Advances in Modeling Earth Systems*, *5*(2), 422–446. doi: 10.1002/jame.20023

Kjellsson, J., Holland, P. R., Marshall, G. J., Mathiot, P., Aksenov, Y., Coward, A. C., ... Ridley, J. (2015). Model sensitivity of the Weddell and Ross seas, Antarctica, to vertical mixing and freshwater forcing. *Ocean Modelling*, *94*, 141–152. Retrieved from https://www.sciencedirect.com/science/article/pii/S1463500315001560 doi: 10.1016/j.ocemod.2015.08.003

Klatt, O., Fahrbach, E., Hoppema, M., & Rohardt, G. (2005, 2). The transport of the Weddell Gyre across the Prime Meridian. *Deep Sea Research Part II: Topical Studies in Oceanography*, *52*(3-4), 513–528. Retrieved from https://linkinghub.elsevier.com/retrieve/pii/S0967064504003066 doi: 10.1016/j.dsr2.2004.12.015

Kuhlbrodt, T., Griesel, A., Montoya, M., Levermann, A., Hofmann, M., & Rahmstorf, S. (2007). On the driving processes of the Atlantic Meridional Overturning Circulation. *Reviews of Geophysics*, *45*, 1–32.

Levitus, S., Boyer, T., Conkright, M., Brien, T., Antonov, J., Stephens, C., ... Gelfeld, R. (1998). *World Ocean Database 1998, Vol. 1, Introduction* (Tech. Rep.). Washington, D.C.: NOAA Atlas NES-DIS 18, U.S. Government Printing Office.

Madec, G., Bourdallé-Badie, R., Bouttier, P.-A., Bricaud, C., Bruciaferri, D., Calvert, D., ... Vancoppenolle, M. (2016, 10). *NEMO ocean engine (version 3.6)* (Tech. Rep.). Retrieved from https://doi.org/10.5281/zenodo.1472492#.XmDJh_JTx4s.mendeley doi: 10.5281/ZENODO.1472492

Matthes, K., Biastoch, A., Wahl, S., Harlaß, J., Martin, T., Brücher, T., ... Park, W. (2020, 6). The Flexible Ocean and Climate Infrastructure version 1 (FOCI1): mean state and variability. *Geoscientific Model Development*, *13*(6), 2533–2568. Retrieved from https://gmd.copernicus.org/articles/13/2533/2020/ doi: 10.5194/gmd-13-2533-2020

Megann, A., & Storkey, D. (2021). Exploring Viscosity Space in an Eddy-Permitting Global Ocean Model: Is Viscosity a Useful Control for Numerical Mixing? *Journal of Advances in Modeling Earth Systems*, *13*(5). doi: 10.1029/2020MS002263

Meijers, A. J. S., Shuckburgh, E., Bruneau, N., Sallée, J.-B., Bracegirdle, T. J., & Wang, Z. (2012). Representation of the Antarctic Circumpolar Current in the CMIP5 climate models and future changes under warming scenarios. *J. Geophys. Res.*, *117*(C12008). doi: 10.1029/2012JC008412

Moat, B., Frajka-Williams, E., Smeed, D., Rayner, D., Johns, W., Baringer, M., ... Collins, J. (2022). *Atlantic meridional overturning circulation observed by the RAPID-MOCHA-WBTS (RAPID-Meridional Overturning Circulation and Heatflux Array-Western Boundary Time Series) array at 26N from 2004 to 2020 (v2020.2)* (Tech. Rep.). British Oceanographic Data Centre - Natural Environment Research Council, UK. doi: 10.5285/e91b10af-6f0a-7fa7-e053-6c86abc05a09

Mohrmann, M., Heuzé, C., & Swart, S. (2021, 9). Southern Ocean polynyas in CMIP6 models. *The Cryosphere*, *15*(9), 4281–4313. Retrieved from https://tc.copernicus.org/articles/15/4281/2021/ doi: 10.5194/tc-15-4281-2021

Morales Maqueda, M. A., Willmott, A. J., & Biggs, N. R. T. (2004, 3). Polynya Dynamics: a Review of Observations and Modeling. *Reviews of Geophysics*, *42*(1). Retrieved from http://doi.wiley.com/10.1029/2002RG000116 doi: 10.1029/2002RG000116

Müller, W. A., Jungclaus, J. H., Mauritsen, T., Baehr, J., Bittner, M., Budich, R., ... Marotzke, J. (2018a). A Higher-resolution Version of the Max Planck Institute Earth System Model (MPI-ESM1.2-HR). *Journal of Advances in Modeling Earth Systems*, *10*(7), 1383–1413. doi: 10.1029/2017MS001217

Müller, W. A., Jungclaus, J. H., Mauritsen, T., Baehr, J., Bittner, M., Budich, R., ... Marotzke, J. (2018b). A Higher-resolution Version of the Max Planck Institute Earth System Model (MPI-ESM1.2-HR). *Journal of Advances in Modeling Earth Systems*, *10*(7), 1383–1413. doi: 10.1029/2017MS001217

Park, W., & Latif, M. (2008, 11). Multidecadal and multicentennial variability of the meridional overturning circulation. *Geophysical Research Letters*, *35*(22), L22703. Retrieved from http://doi.wiley.com/10.1029/2008GL035779 doi: 10.1029/2008GL035779

Rayner, N. A. (2003). Global analyses of sea surface temperature, sea ice, and night marine air temperature since the late nineteenth century. *Journal of Geophysical Research*, *108*(D14), 4407. Retrieved from http://doi.wiley.com/10.1029/2002JD002670 doi: 10.1029/2002JD002670

Reick, C. H., Raddatz, T., Brovkin, V., & Gayler, V. (2013, 7). Representation of natural and anthropogenic land cover change in MPI-ESM. *Journal of Advances in Modeling Earth Systems*, *5*(3), 459–482. Retrieved from http://doi.wiley.com/10.1002/jame.20022 doi: 10.1002/jame.20022

Reintges, A., Martin, T., Latif, M., & Park, W. (2017, 7). Physical controls of Southern Ocean deep-convection variability in CMIP5 models and the Kiel Climate Model. *Geophysical Research Letters*, *44*(13), 6951–6958. Retrieved from http://doi.wiley.com/10.1002/2017GL074087 doi: 10.1002/2017GL074087

Roach, L. A., Dörr, J., Holmes, C. R., Massonnet, F., Blockley, E. W., Notz, D., ... Bitz, C. M. (2020, 5). Antarctic Sea Ice Area in CMIP6. *Geophysical Research Letters*, *47*(9), 1–10. Retrieved from https://onlinelibrary.wiley.com/doi/10.1029/2019GL086729 doi: 10.1029/2019GL086729

Roberts, A., Craig, A., Maslowski, W., Osinski, R., Duvivier, A., Hughes, M., ... Brunke, M. (2015, 7). Simulating transient ice-ocean Ekman transport in the Regional Arctic System Model and Community Earth System Model. *Annals of Glaciology*, *56*(69), 211–228. Retrieved from https://www.cambridge.org/core/product/identifier/S0260305500261417/type/journal_article doi: 10.3189/2015AoG69A760

Roberts, M. J., Baker, A., Blockley, E. W., Calvert, D., Coward, A., Hewitt, H. T., ... Vidale, P. L. (2019, 12). Description of the resolution hierarchy of the global coupled HadGEM3-GC3.1 model as used in CMIP6 HighResMIP experiments. *Geoscientific Model Development*, *12*(12), 4999–5028. Retrieved from https://gmd.copernicus.org/articles/12/4999/2019/ doi: 10.5194/gmd-12-4999-2019

Rodgers, K. B., Aumont, O., Mikaloff Fletcher, S. E., Plancherel, Y., Bopp, L., De Boyer Montégut, C., ... Wanninkhof, R. (2014). Strong sensitivity of Southern Ocean carbon uptake and nutrient cycling to wind stirring. *Biogeosciences*, *11*(15), 4077–4098. doi: 10.5194/bg-11-4077-2014

Savita, A., Kjellsson, J., Kedzierski, R. P., Latif, M., Rahm, T., Wahl, S., & Park, W. (2023). Assessment of Climate Biases in OpenIFS Version 43R3 across

Model Horizontal Resolutions and Time Steps. *Geoscientific Model Development Discussions*, *2023*, 1–25. Retrieved from https://gmd.copernicus.org/preprints/gmd-2023-101/ doi: 10.5194/gmd-2023-101

Scoccimarro, E., Gualdi, S., Bellucci, A., Sanna, A., Fogli, P. G., Manzini, E., ... Navarra, A. (2011). Effects of tropical cyclones on ocean heat transport in a high-resolution coupled general circulation model. *Journal of Climate*, *24*(16), 4368–4384. doi: 10.1175/2011JCLI4104.1

Singh, H. K. A., Landrum, L., Holland, M. M., Bailey, D. A., & DuVivier, A. K. (2021, 3). An Overview of Antarctic Sea Ice in the Community Earth System Model Version 2, Part I: Analysis of the Seasonal Cycle in the Context of Sea Ice Thermodynamics and Coupled Atmosphere-Ocean-Ice Processes. *Journal of Advances in Modeling Earth Systems*, *13*(3). Retrieved from https://onlinelibrary.wiley.com/doi/10.1029/2020MS002143 doi: 10.1029/2020MS002143

Stevens, B., Giorgetta, M., Esch, M., Mauritsen, T., Crueger, T., Rast, S., ... Roeckner, E. (2013). Atmospheric component of the MPI-M earth system model: ECHAM6. *Journal of Advances in Modeling Earth Systems*, *5*(2), 146–172. doi: 10.1002/jame.20015

Storkey, D., Blaker, A. T., Mathiot, P., Megann, A., Aksenov, Y., Blockley, E. W., ... Sinha, B. (2018, 8). UK Global Ocean GO6 and GO7: a traceable hierarchy of model resolutions. *Geoscientific Model Development*, *11*(8), 3187–3213. Retrieved from https://www.geosci-model-dev.net/11/3187/2018/ doi: 10.5194/gmd-11-3187-2018

Swart, N. C., & Fyfe, J. C. (2012). Observed and simulated changes in the Southern Hemisphere surface westerly wind-stress. *Geophysical Research Letters*, *39*(16). doi: 10.1029/2012GL052810

Treguier, A. M., Held, I. M., & Larichev, V. D. (1997, 4). Parameterization of Quasigeostrophic Eddies in Primitive Equation Ocean Models. *Journal of Physical Oceanography*, *27*(4), 567–580. Retrieved from http://journals.ametsoc.org/doi/abs/10.1175/1520-0485%281997%29027%3C0567%3APOQEIP%3E2.0.CO%3B2 doi: 10.1175/1520-0485(1997)027⟨0567:POQEIP⟩2.0.CO;2

Turner, J., Bracegirdle, T. J., Phillips, T., Marshall, G. J., & Scott Hosking, J. (2013). An initial assessment of antarctic sea ice extent in the CMIP5 models. *Journal of Climate*, *26*(5), 1473–1484. doi: 10.1175/JCLI-D-12-00068.1

Voldoire, A., Saint-Martin, D., Sénési, S., Decharme, B., Alias, A., Chevallier, M., ... Waldman, R. (2019, 7). Evaluation of CMIP6 DECK Experiments With CNRM-CM6-1. *Journal of Advances in Modeling Earth Systems*, *11*(7), 2177–2213. Retrieved from https://onlinelibrary.wiley.com/doi/abs/10.1029/2019MS001683 doi: 10.1029/2019MS001683

Wang, C., Zhang, L., Lee, S.-K., Wu, L., & Mechoso, C. R. (2014). A global perspective of CMIP5 climate model biases. *Nat. Climate Change*, *4*, 201–205. doi: 10.1038/NCLIMATE2118

Wang, Y., Heywood, K. J., Stevens, D. P., & Damerell, G. M. (2022). Seasonal extrema of sea surface temperature in CMIP6 models. *Ocean Science*, *18*(3), 839–855. doi: 10.5194/os-18-839-2022

Williams, K. D., Copsey, D., Blockley, E. W., Bodas-Salcedo, A., Calvert, D., Comer, R., ... Xavier, P. K. (2018, 2). The Met Office Global Coupled Model 3.0 and 3.1 (GC3.0 and GC3.1) Configurations. *Journal of Advances in Modeling Earth Systems*, *10*(2), 357–380. Retrieved from https://onlinelibrary.wiley.com/doi/abs/10.1002/2017MS001115 doi: 10.1002/2017MS001115

Yamamoto, A., Abe-Ouchi, A., & Yamanaka, Y. (2018). Long-term response of oceanic carbon uptake to global warming via physical and biological pumps. *Biogeosciences*, *15*(13), 4163–4180. doi: 10.5194/bg-15-4163-2018